

An image-based equation for estimating the prospective CO₂ storage resource of organic-rich shale formations

Alexander Azenkeng^{a,*}, Blaise A.F. Mibeck^a, Bethany A. Kurz^a, Charles D. Gorecki^a, Evgeniy M. Myshakin^{b,c}, Angela L. Goodman^b, Nicholas A. Azzolina^a, Kurt E. Eylands^a, Shane K. Butler^a, Sean Sanguinito^{b,c}

^a University of North Dakota, Energy & Environmental Research Center, 15 North 23rd Street Stop 9018, Grand Forks, ND 58202-9018, USA

^b U.S. Department of Energy, National Energy Technology Laboratory, 626 Cochrans Mill Road, Pittsburgh, PA 15236, USA

^c Leidos Research Support Team, 626 Cochrans Mill Road, Pittsburgh, PA, USA



ARTICLE INFO

Keywords:
Image analysis
Volumetric equation
CO₂ storage estimates
Organic-rich shales

ABSTRACT

An image-based volumetric equation for estimating the prospective CO₂ mass storage resource potential for organic-rich shale formations has been developed using data obtained from advanced image analysis of Bakken Formation shale samples. The equation is a modification of the U.S. Department of Energy (DOE) National Energy Technology Laboratory's (NETL's) volumetric equation methodology for estimating the prospective CO₂ mass storage resource for shale formations. The current equation enhances DOE's version by systematically deriving expressions for calculating efficiency factors based on analysis of high-resolution field-emission scanning electron microscopy (FESEM) shale images. FESEM images are used to obtain improved nanoscale porosity estimates for the shale matrix and OM. The calculation of the efficiency factors associated with free-phase storage and CO₂ adsorption onto solid surfaces are based on a ratio of connected-to-nonconnected porosity and the newly developed shared border analysis (SBA) method, respectively. The image-based equation described herein is structured so that it can be adapted and applied to other formation types by considering the specific mineralogy or matrix characteristics. Preliminary data used to illustrate the newly developed equation show that the Upper Bakken Shale (UBS) may have a lower prospective CO₂ storage resource potential than the Lower Bakken Shale (LBS) by about 65 %. Although these results are neither optimized for each lithofacies nor represent the Bakken formation regional scale, they are encouraging for unfractured shale samples and serve as a useful starting point for future evaluations at the regional scale.

1. Introduction

Carbon capture and storage (CCS) technologies are currently at various stages of development for the primary purpose of reducing anthropogenic CO₂ emissions to curtail the effects that greenhouse gases such as CO₂ can have on global warming. Bachu et al. (2007) have reviewed the progress made in assessing CO₂ storage opportunities in various subsurface geologic media, including depleted oil and gas reservoirs, unminable coal beds, and deep saline aquifers, as well as a detailed discussion of pertinent CO₂ storage mechanisms. The most notable advances in CO₂ storage efforts include commercial-scale CO₂ injection projects around the world such as Sleipner (Furre et al., 2017) and Snøhvit (Shi et al., 2013) in Norway, Weyburn-Midale (Preston et al., 2005; Petroleum, 2019) in Canada, Salah (Ringrose et al., 2013) in Algeria, and Salt Creek (Hendricks, 2009; Norris et al., 2014) in the

United States. Improvements in directional drilling technology (Watney, 2016) and hydraulic fracturing (King, 2010) of organic-rich shale and other tight rock formations have opened new opportunities for CO₂ storage, with the potential co-benefit of enhancing gas and oil recovery. As a result, shale formations that have been previously viewed mostly as CO₂ storage seals to the conventional geologic media are now being considered as an emerging potential CO₂ storage resource, especially organic-rich shales with total organic carbon (TOC) content of at least 2 wt% (Goodman et al., 2014; Levine et al., 2016).

Although significant progress has been made to investigate the suitability of subsurface geologic sinks for CO₂ storage (Preston et al., 2005; Torp and Gale, 2004; Chadwick et al., 2004; Hamling et al., 2013), estimating the storage resource of emerging shale reservoirs faces serious challenges. One of the unresolved difficulties with organic-rich shale formations is the lack of detailed geologic and petrophysical

* Corresponding author.

E-mail address: aazenkeng@undeerc.org (A. Azenkeng).

data that are needed to develop improved volumetric equations for assessing the CO₂ storage resource potential. According to the DOE NETL method for estimating regional-scale CO₂ storage resources, the key factors that control CO₂ storage in geologic formations include porosity within induced fractures, natural fractures, and matrix pores as well as the occurrence and distribution of kerogen and clay minerals (Goodman et al., 2014). In organic-rich shales, it is difficult to differentiate between free-phase CO₂ storage in induced fractures, natural fractures, or matrix pore spaces. As a result, the free-phase volume due to matrix porosity and fractures is often grouped into a single void volume parameter in the equation used to estimate the CO₂ mass storage resource for organic-rich shale formations. Similarly, the capacity of the solid fraction of the shale to adsorb CO₂ is described by a parameter that groups the adsorption capacity of clay minerals and kerogen as representatives of inorganic and organic matter, respectively.

In conventional reservoirs, efficiency factors that describe the ability of CO₂ to access available pore spaces can be derived from core analysis data and estimated from oil and gas recovery factors. For unconventional shale reservoirs, petrophysical parameters such as porosity, pore size distributions, and adsorption capacity estimates can be derived from core measurements; however, most of the shale adsorption measurements are made on crushed samples which ignore pore network interconnectivity, thus, the technique provides values which represent the maximum potential CO₂ uptake in a sample. The new non-destructive, image-analysis method described herein provides the possibility to refine the adsorption contribution measurements by accounting for accessibility of CO₂ in the pore spaces of the solids. To address the challenges of estimating the CO₂ storage resource potential in low porosity, low permeability reservoirs, new approaches are needed to better estimate total void volume fractions and adsorption capacities of all adsorptive components in the shale matrix. Additionally, efficiency factors that account for the ability of CO₂ to access the available void spaces and for adsorption onto clay or OM particles would be required for improved assessment of the prospective CO₂ mass storage resource capacity using volumetric approaches.

In this study, an image-based equation has been developed that provides robust formulations for calculating efficiency factors using data obtained from advanced image analysis of high-resolution FESEM images of Bakken Formation shale samples. The equation presented herein focuses on the two key CO₂ storage mechanisms for organic-rich shales, namely, free-phase storage in void spaces and CO₂ adsorption onto surfaces of OM and clays. The equation is also structured so that other potential CO₂ uptake mechanisms, such as geochemical reactions with formation minerals, can be fully incorporated if appropriate formulations are derived. As a result, the equation can be applied more generally to any reservoir for the purpose of estimating the prospective CO₂ mass storage resource potential using a combination of image analysis and laboratory-derived experimental data.

2. Geologic CO₂ storage mechanisms in organic-rich shale formations

Generally, subsurface CO₂ storage mechanisms can be divided into physical and chemical trapping processes, with a combination of the two more likely to occur in most cases (Bachu et al., 2007; Intergovernmental Panel on Climate Change, 2005). Physical trapping occurs when CO₂ is immobilized as free gas or supercritical fluid in stratigraphic and structural traps or as residual gas trapped in the pore/fracture space at irreducible gas saturation. Chemical trapping occurs when CO₂ dissolves in formation fluids and may then be involved in precipitation reactions with the rock matrix or becomes adsorbed onto mineral surfaces such as clays and solid OM. The two broad categories of mechanisms (physical and chemical) can be further classified as free-phase storage in formation/reservoir void spaces because of pores and fractures, adsorption onto the surfaces of minerals or OM that have strong attraction with CO₂, absorption within porous OM, solubility in

formation fluids, and mineralization reactions. These mechanisms have a strong dependence on factors such as reservoir characteristics, flow behaviors, and CO₂ properties at different reservoir temperature and pressure. Reaction kinetics and timescales are also important considerations that help to determine the ultimate fate of CO₂ in the reservoir. Hence, derivation of equations for estimating the CO₂ mass storage resource capacity of a given formation/reservoir must take into account the relevant mechanisms that may be applicable in a given geologic unit.

Shale matrices with low porosity and low permeability, are limited with respect to the amount of CO₂ that can be stored via physical trapping mechanisms. However, improvements in technologies for hydraulic fracturing of hydrocarbon-rich shale formations have turned such formations into potential CO₂ storage targets: with the co-benefit of enhanced oil or gas recovery. Hydraulic fracture stimulation helps to provide migration pathways for CO₂ to reach a greater extent of the formation and can facilitate CO₂ migration into unfractured portions of the rock matrix.

CO₂ adsorption onto solid particle/grain surfaces is a major storage mechanism in shales, especially those that are rich in OM (i.e., ≥ 2 wt %). Several studies have investigated CO₂ adsorption as a primary storage mechanism in shales (Busch et al., 2008; Chareonsuppanimit et al., 2012; Liu et al., 2013; Tao and Clarenz, 2013). In general, these studies suggest that high total organic carbon (TOC) content is a critical parameter for appreciable CO₂ adsorption potential in organic-rich shales. However, other studies have also shown that additional factors such as the presence of clay minerals can contribute to CO₂ adsorption in shale matrices (Chareonsuppanimit et al., 2012; Busch et al., 2008). Specifically, Busch et al. (2008) have reported a significant CO₂ storage potential (about 97 times better than coal and about 38 times better than connected sandstone) in an Australian Muderong shale with TOC content of < 0.5 wt%. In that shale, high CO₂ adsorption can be attributed to a large smectite content (~ 20 wt%), swelling clays capable to capture CO₂ into the interlayer space (Myshakin et al., 2013). These CO₂ adsorption studies suggest that both OM and clay minerals are the dominant adsorption components for CO₂ adsorption storage mechanisms in organic-rich shales. For the Bakken formation shales, the OM content can be as high as 30 wt% and the clay content can reach 60 wt% or higher in some places (Lei, 2016). However, these concentrations of OM and clay can vary both by depth and by lateral location in the Williston Basin. Thus, CO₂ adsorption onto OM and clay surfaces potentially accounts for a significant portion of the prospective CO₂ storage quota.

The extremely tight pore spaces in organic-rich shales practically limit the feasibility of solubility mechanisms, where CO₂-laden fluids in pore spaces would have to be replaced continuously by "fresh" formation fluids based on equilibrium and buoyancy considerations. Similarly, mineralization requires reaction with formation minerals such as alkali silicates or a significant presence of carbonates that can be involved in dissolution/precipitation reactions. However, the lack of high carbonate content in organic-rich shales as a result of deposition in oxygen-deprived marine environments limits dissolution/precipitation mechanisms. Considering these limitations with some of the CO₂ uptake mechanisms in organic-rich shales, this work focused more on deriving expressions for estimating free-phase storage in pores and fractures as well as solid-phase storage primarily on OM and clay surfaces. The derived CO₂ storage resource equation also provides the flexibility to include contributions from other CO₂ uptake mechanisms when the appropriate formulations become available and if the additional mechanisms are determined to be significant. The component-by-component structure of the equation also allows for a more general application of the equation to other formations with a mineral composition that is different from that of organic-rich shale formations.

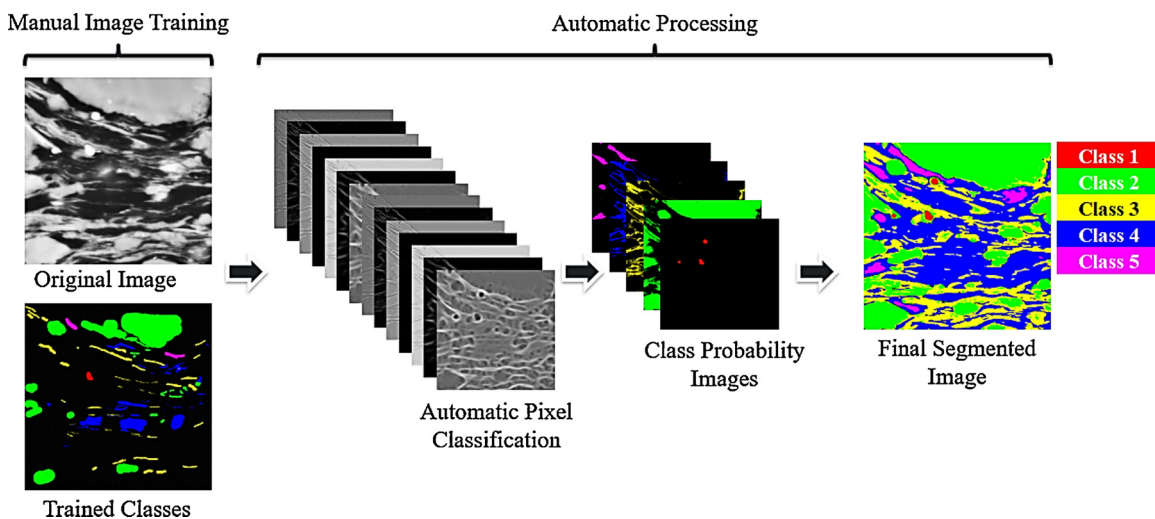


Fig. 1. Workflow of Ilastik segmentation for shale and tight rock characterization.

3. Concept of image-based volumetric equation

The underlying concept of an image-based approach was to apply advanced image analysis protocols to high-resolution FESEM images to derive important scaling or efficiency factors for improved estimates of the prospective CO₂ mass storage resource potential for organic-rich shale formations. The efficiency factors were computed using data obtained from images by a newly developed technique, referred to as the shared border analysis (SBA) method (discussed later). The overall goal was to obtain a mathematical expression that enables quantitative estimates in a rather generalized equation that can be applied to any formation. The data used in the equation contain characteristics and properties that are specific to an organic-rich shale reservoir but can be easily adapted to other reservoir types. In addition, the image-based formulation provides the flexibility to include/exclude additional terms that may be necessary/unnecessary depending on the determined CO₂ transport and trapping mechanisms for a specific reservoir. To the best of our knowledge, this is the first time these efficiency factors (also known as formation factors, capacity factors or capacity coefficients) have been robustly calculated by image analysis techniques to include reservoir-specific properties and characteristics such as mineralogy and the availability of the matrix components (minerals and/or OM) to contact CO₂ within pores or fractures.

Although the results presented herein as an illustration of the newly developed equation are exciting, they are based on 40 image frames acquired on each of the six shale samples, 3 UBS and 3 LBS, from 3 select locations (NDIC Well 22388, 16974, and 18829) of the Bakken Formation. These locations were selected to represent areas where the source rock is considered thermally mature (Well 22388), marginally mature (Well 16974), and immature (Well 18829) relative to the oil window. A more extensive study involving a larger sample set covering more areas of the Bakken Formation would be needed to expand and apply this method to better estimate representative efficiency factors and the prospective CO₂ storage resource potential for the Bakken Formation shale at the regional scale. Such an expanded study is also necessary to capture the highly variable lithofacies heterogeneities that are a common occurrence in the Bakken shales.

3.1. Advanced image analysis protocol

High-resolution images acquired by FESEM were processed by an advanced image analysis approach that utilized a combination of image analysis programs, including Ilastik (Sommer et al., 2011), Image-J (Rasband, 2016), and Fiji (Schindelin et al., 2012). In particular, the Ilastik program has built-in advanced capabilities for efficient

segmentation of the image features based on several attributes such as texture, shape, and grey scale. Hence, high resolution images with high feature contrast and detailed micro-texture are critical for optimal and efficient segmentation. Two sets of images were acquired for each sample to improve the spatial resolution of different pores or features in the tight rock matrix and within the OM particles. The first set of images was obtained at a magnification of about 3000x (LowMag) and a second set was obtained at about 20,000x or a suitable higher magnification (HighMag). A total of 40 images were analyzed for each sample at 3000x and the number of images analyzed at 20,000x depended on the number of distinct OM particles that were observed within the area scanned at 3000 × . Specifically, there were 11 images for the UBS and 3 images for the LBS for the marginal maturity core; 3 images for UBS and 14 images for the LBS for the immature core; and, 14 images for the UBS and 15 images for the LBS for the mature core. The scan area for each LowMag image was 1344 μm² and the area of each HighMag image was 30 μm², with pixel resolutions of 16.5 nm and 2.5 nm for the LowMag and HighMag images, respectively. The higher resolution of 2.5 nm at 20,000 × (i.e., by zooming into the particle) was necessary to spatially resolve nanometer size pores within the OM particles. It should be noted that these limited sets of images are only used to help illustrate the proposed image-based equation approach presented herein and, thus, not a complete representation of Bakken shale heterogeneity.

LowMag images were used to quantify void space (pores and fractures), OM, clays, medium density minerals (MDmin), and high density minerals (HDmin) at the microscale, while the HighMag images were used primarily to segment and quantify void space and features at the nanoscale such as porosity associated with OM (PAOM). For clarification, MDmin refers to major mineral types such as quartz, calcite, dolomite, K-feldspar, etcetera that do not have high atomic number elements, while HDmin includes primarily pyrite and occasionally zircon or monazite which contain high atomic number elements. The LowMag images were acquired in a random manner to increase the chances of collecting a set of images that was representative of the sample matrix and free from bias. Because a key goal of collecting the HighMag images was to evaluate PAOM, the collection of those images was focused on OM particles in the sample matrix. After applying a magnification correction, the total porosity for each sample was obtained by summing the LowMag porosity and HighMag porosity.

A workflow developed for segmenting the images is shown in Fig. 1. The FESEM images were imported into Ilastik and the program was trained to segment the images into different classes representing different features of interest. As part of the segmentation process, the Ilastik program uses complex information about the image such as

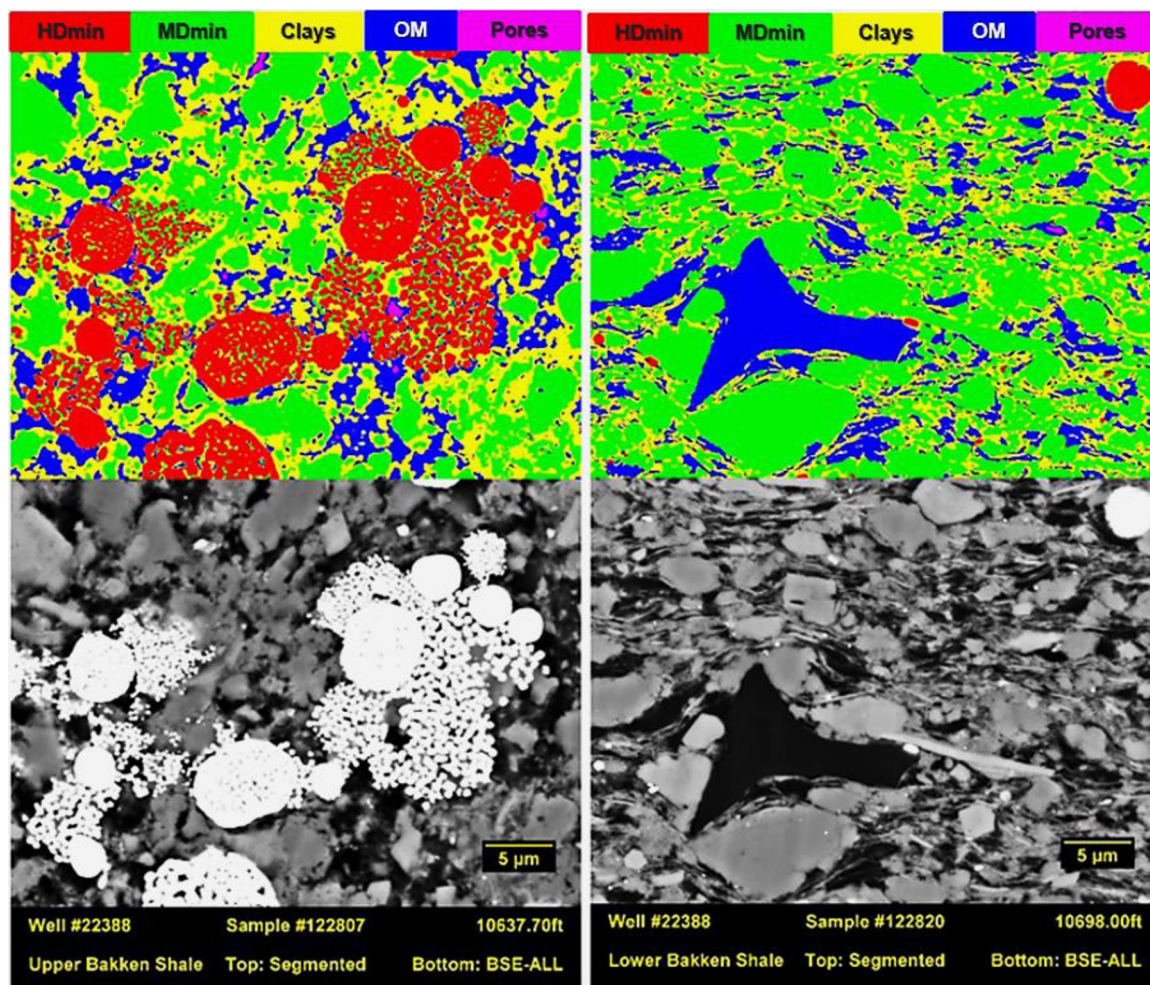


Fig. 2. Illustration of finalized Ilastik segmentation images and the corresponding grey scale versions for UBS (left) and LBS (right) samples.

texture, shape, and grey scale. In addition, mathematical algorithms using functions such as Gaussian blur and probabilistic approaches are used to obtain class probability images on a pixel-by-pixel basis that are then merged to obtain a final version of the segmented image. The ability of Ilastik to not only perform pixel level classification, but to also incorporate micro-texture characteristics and small grey scale variations within the matrix features is critical for shale characterization due to the fine-grained nature of the material. Fig. 2 shows an example of FESEM images and their corresponding segmented versions for UBS and LBS images obtained from samples collected from a thermally mature (within the oil window) location of the Bakken.

3.2. Specific feature masks

To separate and quantify specific features such as PAOM and clay minerals, an additional process involving creation of specific masks for OM, clay particles, and pores was developed. This process was also useful for quantifying nanoscale fractures within OM particles. Pores and fractures within OM are important for estimating the total void volume fraction, which is important for computing the prospective CO₂ mass storage resource potential for shale and other tight rock reservoirs. The steps involved in the creation of OM, clay, and pores masks are depicted in Fig. 3 and briefly described below.

3.2.1. OM mask

A local contrast enhancement was performed on the original FESEM image and an automatic threshold, using the Otsu method (Otsu, 1979) implemented in Image-J, was applied to separate OM with its

embedded clay particles from the rest of the matrix. The resultant image was then binarized and cleaned by additional image filters to obtain the OM mask. The threshold used to separate different rock matrix components based on brightness/contrast values includes pores < 1000, OM in the range 1000–27,000, and clays > 27,000.

3.2.2. Clay mask

A clay mask was obtained by applying the OM mask to an enhanced FESEM image to obtain an image of just OM matrix and embedded clays. A manual threshold was applied to the OM/clays image to separate clay particles from OM matrix. The resultant image was then binarized and cleaned to create a clay mask.

3.2.3. Pore mask

A pore mask was created by applying the clay mask to the OM/clays image to obtain an image of just the OM matrix and pores. A manual threshold was then applied to the OM/pores image to separate pores from the OM matrix. The resultant image was then binarized and cleaned to create a pore mask.

To evaluate the quality of the feature masks and how well they delineate the various particle types within the OM matrix, especially nanopores, the individual feature masks were combined and overlaid on the original FESEM image for comparison. The OM, clay, and pore masks were assigned to the red, green, and blue channels, respectively, to obtain a composite RGB image of the masks. The RGB composite image was then reduced to edges of different features and overlaid onto the original FESEM image for comparison. A zoomed section of the comparison image in Fig. 4 shows good agreement in the resolution of

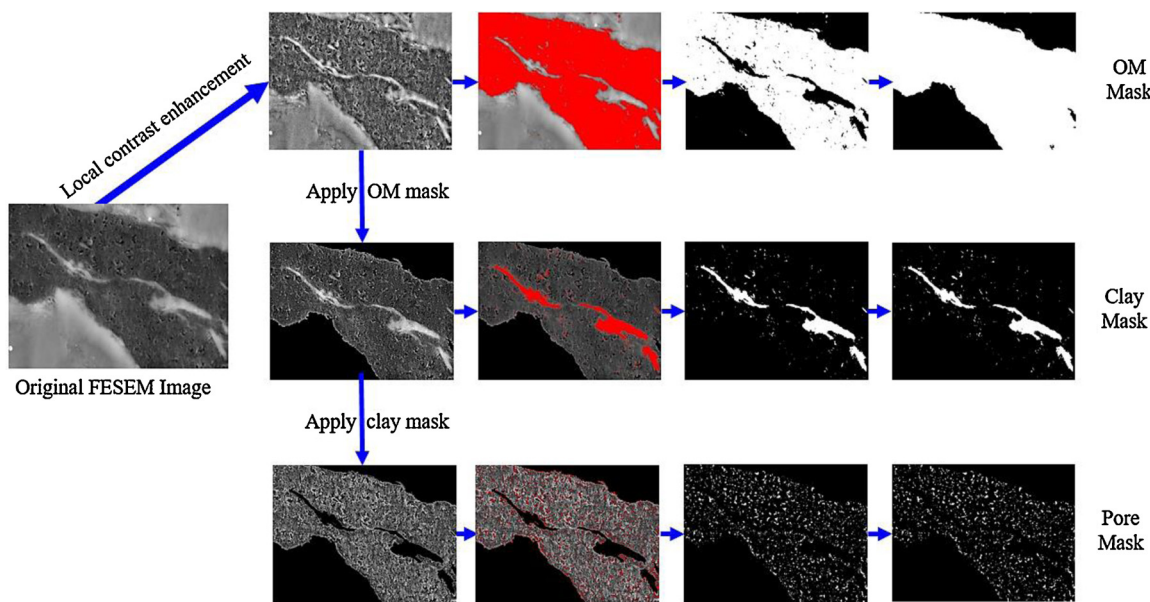


Fig. 3. Illustration of the process for creating specific feature masks.

pores and clays within the OM matrix.

3.3. Shared border analysis

A shared border analysis (SBA) approach was developed based on the advance image analysis results for the purpose of estimating efficiency factors for the adsorption of CO_2 onto clay and OM particles in the shale matrix. As discussed earlier, adsorption onto OM and clay mineral surfaces is expected to constitute the dominant CO_2 adsorption mechanisms in organic-rich shales. Hence, the principle of SBA is based on the fact that CO_2 adsorption onto OM or clay mineral surfaces can only occur if that surface is exposed to connected pore or fracture space within the shale matrix and, thus, accessible to CO_2 . In other words, the

surface shares a border with interconnected pore/fracture space. However, because OM or clay mineral particles may not necessarily be surrounded entirely by the pore space, only a fraction of the circumference that is exposed to a connected pore/fracture space can adsorb CO_2 .

Fig. 5 shows a schematic illustration of the SBA process for obtaining feature classes from a segmented image and for computing the shared border segment or fraction between any two classes such as OM and pore or clay and pore. Briefly, the original FESEM image undergoes advanced image analysis and segmentation described earlier. A binary image is created for each class (white) of interest, while all others are turned into background (black). The pore or OM class particles are then dilated by one pixel and a Boolean AND is used to obtain the

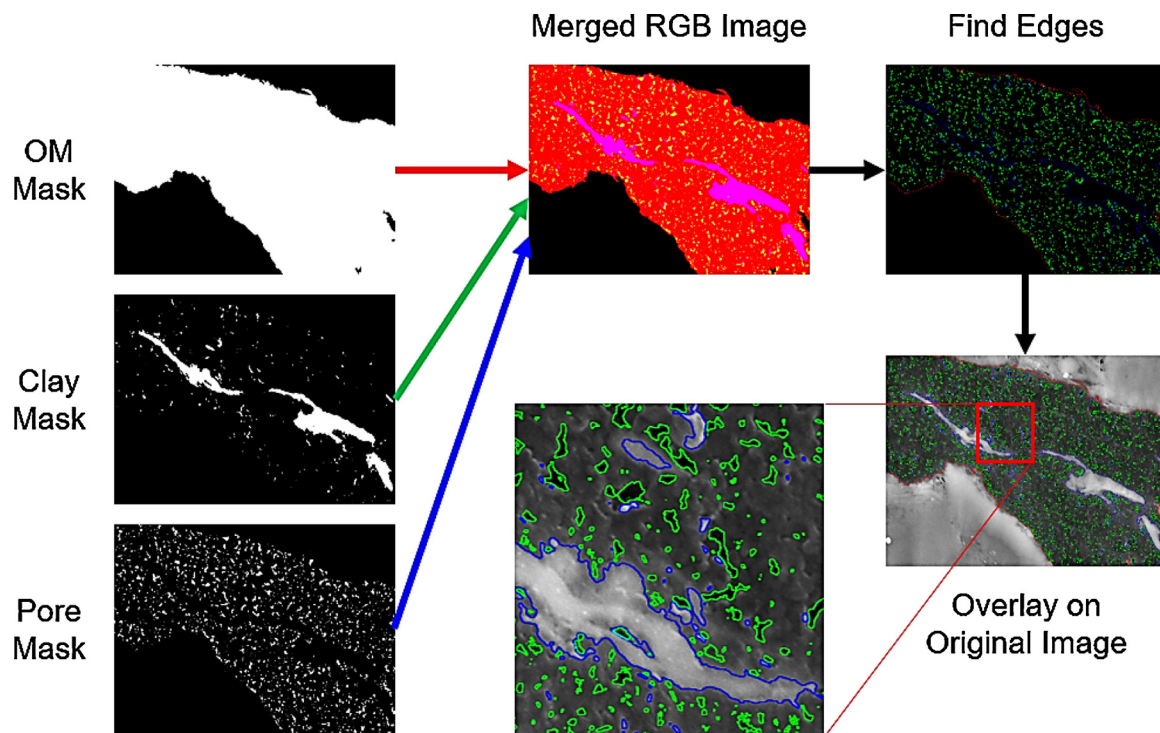


Fig. 4. Verification of the quality of specific feature masks.

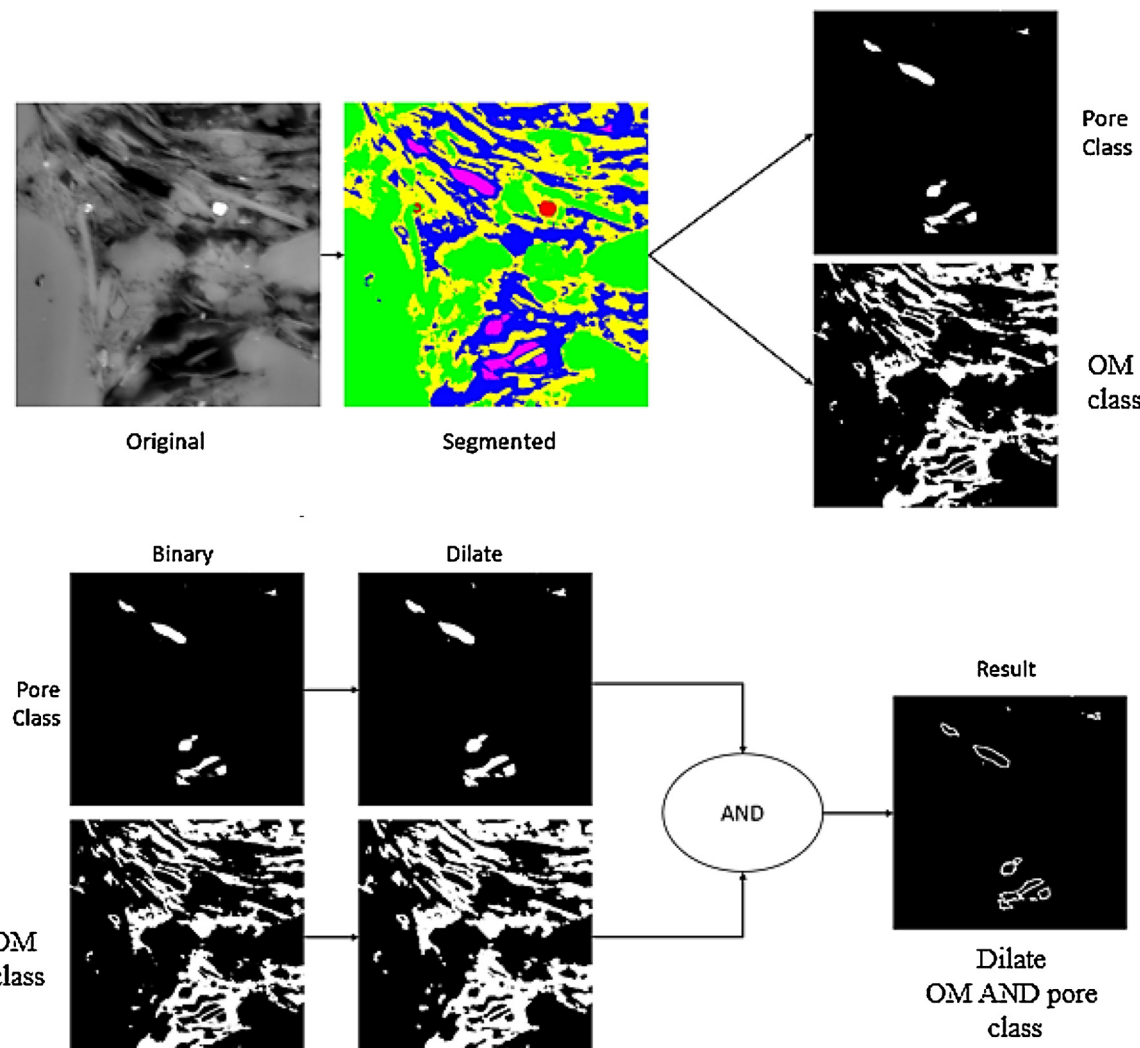


Fig. 5. Schematic illustration of shared border analysis.

overlapping pixels. A skeletonizing filter is applied to remove the dilated pixels and the image frame edges are turned into background (black) to avoid addition of image edge effects to the shared borders. The remaining one pixel thick features represent the shared border pixels that are counted. The number of shared border pixels is divided by the total number of pixels in the circumference of the particle to obtain a fraction of shared border, which is used as an estimate of the OM or clay particle surface available for CO₂ adsorption. An ImageJ macro/routine was implemented to perform the sequences illustrated in Fig. 5 and to calculate the shared border segments. The routine computes the average of the shared border segments in a given image and the overall average over all images processed for a given sample to obtain the efficiency factors for CO₂ adsorption onto OM or clay minerals surfaces described later.

4. Proposed CO₂ mass storage resource estimation equation

Advanced image analysis (AIA) methods were used to determine geochemical and petrophysical parameters such as total porosity fraction and fraction of each mineral component in Bakken formation shale samples. Additionally, AIA techniques facilitated estimation of efficiency factor expressions using the newly introduced SBA approach. These parameters were combined to derive an overall image-based volumetric equation for estimating the prospective CO₂ mass storage potential for organic-rich shales from the Bakken formation. The

equation described herein is a modification of DOE NETL's volumetric equation methodology for estimating the prospective CO₂ mass storage resource for shale formations (Goodman et al., 2014; Levine et al., 2016), which is given by:

$$G_{CO_2} = V_e [\rho_{CO_2} \phi E_\phi + \rho_{sCO_2} (1 - \phi) E_s] \quad (1)$$

where G_{CO_2} = CO₂ mass storage resource of the shale formation, V_e = Net effective volume of the formation, ρ_{CO_2} = Density of CO₂ at reservoir temperature and pressure prior to production, ϕ = Percentage of bulk volume that is void, E_ϕ = Fraction of shale porosity within V_e available for CO₂ storage, ρ_{sCO_2} = Maximum mass of CO₂ sorbed per unit volume of solid rock, E_s = Fraction of total potential sorbed volume of CO₂ within V_e .

Eq. 1 contains two main CO₂ storage contributions from void volume spaces (free phase) and solid phase (via adsorption) which account for the two main CO₂ storage mechanisms for shale formations. The volume of formation that can effectively be accessed for CO₂ storage, V_e , is given by

$$V_e = A_t E_A h_g E_h \quad (2)$$

where A_t is the total area of the shale formation being assessed for CO₂ storage, E_A is the fraction of shale formation total area available for CO₂ storage, h_g is the total thickness of the shale formation, and E_h is the fraction of shale formation gross thickness available for CO₂ storage. The formation area efficiency factor, E_A , represents a reduction in

available storage resource area as viewed on a map of the shale after eliminating acreage because of social or physical geological restrictions (Rodosta et al., 2011). The formation thickness efficiency factor, E_h , represents limits placed on the shale storage resource because of formation-scale characteristics that change as a function of depth. This efficiency is dependent on vertical changes in geologic properties and characteristics of the formation such as lithology, permeability, porosity, fracture density, and fracture connectivity that create a less favorable environment for oil and gas exploitation, thus effectively precluding later CO₂ injection (Levine et al., 2016). In this study, the effective formation volume term given above was used in its original formulation (Levine et al., 2016; Goodman et al., 2014) without any further modification.

The advanced mineral identification and characterization system (AMICS) software (Gloy, 2019; Bruker, 2019) was used to quantify the mineralogy (including OM) on a particle-by-particle or grain-by-grain basis for a total of 40 image frames for each sample. Each frame covered an area of only 85 μm by 85 μm, thus, given the mineralogical and morphological variation seen in many shale samples, and given the small area of the sample represented by the 40 frames, additional image collection and processing would be required to characterize each sample in a statistically-valid manner. The goal of this work was to develop and demonstrate the methodology, not to calculate statistically-valid estimates of the potential CO₂ storage resource within the Bakken. Mineral phase classifications were aided by the chemical compositions obtained from the energy-dispersive x-ray spectroscopy (EDS) detector that was coupled to the FESEM system. Based on data obtained from AMICS, AIA, and SBA, Eq. 1 was modified as follows:

$$G_{CO_2} = V_e [\rho_{CO_2} \phi_{tot} E_\phi + M_{OMCO_2} F_{OM} E_{OM} + M_{ClaysCO_2} F_{Clays} E_{Clays} + Others] \quad (3)$$

where G_{CO_2} = CO₂ mass storage resource (kg), V_e = Effective reservoir volume (m³), ρ_{CO_2} = Density of CO₂ at reservoir temperature and pressure (kg/m³), ϕ_{tot} = Total free phase void volume fraction (m³/m³), E_ϕ = Efficiency factor for free phase storage (m³/m³), F_{OM} = Fraction of V_e occupied by solid OM particles (m³/m³), M_{OMCO_2} = Maximum mass of CO₂ adsorbed per unit volume of solid OM (kg/m³), E_{OM} = Efficiency factor for adsorption of CO₂ on OM particles (m/m), F_{Clays} = Fraction of V_e occupied by clay mineral particles (m³/m³), $M_{ClaysCO_2}$ = Maximum mass of CO₂ adsorbed per unit volume of clays (kg/m³), E_{Clays} = Efficiency factor for adsorption of CO₂ on clay particles (m/m), $Others$ = Contribution from other potential CO₂ uptake mechanisms (kg/m³)

4.1. Efficiency factor for free phase storage, E_ϕ

From Eq. (3), the efficiency factor E_ϕ is and fractures, that is accessible to CO₂ for free phase storage. In this study, E_ϕ was expanded to include two terms: $E_{\phi eff}$, which is the ratio of connected-to-total void volume and E_D , which is the reservoir fluid displacement efficiency. The definition of $E_{\phi eff}$ effectively excludes any void spaces that are not accessible to CO₂ because of lack of connectivity and is a simple calculation of connected porosity (ϕ_{con}) divided by total porosity (ϕ_{tot}). Porosity used in this context expressly includes void space contribution from matrix fractures as well. The displacement efficiency term accounts for the fact that existing fluids in the connected void spaces in the reservoir have to be displaced during CO₂ injection to create the net void space that can store CO₂. E_D (IEAGHG, 2014) is further divided into a volumetric displacement efficiency (E_{vol}) and microscopic displacement efficiency (E_d). Volumetric displacement efficiency describes the fraction of void volume contacted by CO₂ from the injection well as a result of density difference between the injected CO₂ and formation fluids. Microscopic displacement efficiency represents the actual fraction of void spaces available for CO₂ storage excluding any irreducible oil (S_{oil}) and/or water (S_{wirr}) saturation. Therefore, E_ϕ can be computed

as follows:

$$E_\phi = E_{\phi eff} E_D \quad (4)$$

$$E_{\phi eff} = \frac{\phi_{con}}{\phi_{tot}} \quad (5)$$

$$E_D = E_{vol} E_d \quad (6)$$

$$E_d = 1 - S_{wirr} - S_{oil} \quad (7)$$

The calculation of E_ϕ presented herein is a step toward an improved estimate over conventional methods for organic-rich shales by accounting for factors such as fluid displacement in the reservoir rock matrix. Until data become available from field deployment of CO₂ storage in shale reservoirs, the estimation of reservoir fluid displacement efficiency will likely occur through laboratory-based tests and/or reservoir modeling. The determination of connected versus non-connected porosity can be achieved by using advanced porosity measurement techniques developed for shales, such as pressure pulse decay (Gilicz and Bodai, 2012), which is a direct measurement of connected (or accessible) porosity. To further understand void space breakdown into pores versus fractures, advanced image analysis techniques were employed. Additional image analysis-based methods are being explored and developed to further differentiate between connected versus non-connected fractures and pores. Once these methods are developed, it will greatly help to expand our current knowledge of fluid flow mechanisms in tight reservoirs and help to better understand the adsorptive components that CO₂ could contact as it migrates through the reservoir.

4.2. Efficiency factors for CO₂ adsorption onto OM, E_{OM} , and clays, E_{Clays}

The efficiency factors for CO₂ adsorption onto OM and clay particles were computed from AIA protocols and the SBA approach described earlier. Briefly, the calculation of adsorption efficiency factors for each relevant mineral component entails a series of SBA steps illustrated using OM particles as follows:

- 1 The length of an OM particle border shared with or exposed to a connected pore or fracture space is computed and normalized to the total border surrounding the particle.
- 2 The average of the normalized shared borders over all OM particles in the image is determined.
- 3 An overall average of normalized shared borders computed over all images obtained for a given sample is used as an estimate of the efficiency factor associated with CO₂ adsorption onto OM for the sample.

The process outlined in Steps 1–3 is repeated for each component that can potentially adsorb CO₂ to obtain an estimate of the efficiency factor associated with adsorption of CO₂ on particles of that component for a given sample. Thus, the equations for calculating E_{OM} and E_{Clays} are given by:

$$E_{OM} = \frac{1}{M} \sum_{i=1}^M \frac{1}{N} \sum_{j=1}^N \frac{\delta_{(OM-P)ij}}{C_{(OM)ij}} \quad (8)$$

and

$$E_{Clays} = \frac{1}{M} \sum_{i=1}^M \frac{1}{N} \sum_{j=1}^N \frac{\delta_{(Clays-P)ij}}{C_{(Clays)ij}} \quad (9)$$

where M is the total number of images analyzed per sample, N is the total number of OM or clay particles analyzed per image, $\delta_{(OM-P)ij}$ is the length of OM border accessible to CO₂ shared with pores or fractures for OM particle j in image i, $C_{(OM)ij}$ is the circumference of OM particle j in image i, $\delta_{(Clays-P)ij}$ is the length of clay particle border accessible to CO₂ shared with pores or fractures for clay particle j in image i, and $C_{(Clays)ij}$

is the circumference of clay particle j in image i . The calculation of E_{OM} and E_{Clays} by the SBA approach effectively removes OM and clay portions included in F_{OM} and F_{Clays} that may never be exposed to CO_2 for adsorption.

Clay minerals demonstrate different affinity for CO_2 adsorption like that in the interstratified illite-smectite sequences that can be found in shales. Smectites as swelling clays can potentially accommodate CO_2 in the interlayer space of the structural units. This represents a phenomenon that cannot be captured by image analysis, because interlayer spaces are within the clay particle structures. Although this potential CO_2 uptake fraction is not included in the current formulation of the equation, its impact on the estimations made by the proposed equation is expected to be important only to limited cases of smectite-rich shales.

4.3. Fraction of organic matter, F_{OM} , and clays, F_{Clays}

The fractions of OM and clays within the effective reservoir volume were determined using AMICS software, where a combination of FESEM backscattered electron (BSE) images and x-ray chemical composition data are used to derive the mineralogy on a particle-by-particle or grain-by-grain basis. Within the AMICS software, the fraction of each mineral component (including total porosity and OM) can be calculated based on a stereological volume approximation (Gundersen and Jensen, 1987; Howard and Reed, 1998; Weibel, 1979), where the sum of 2-D areas determined from image analysis is proportional to the volume. Therefore, the fractions of a sample volume taken by OM, F_{OM} , and by clays, F_{Clays} , shown in the second and third terms of Eq. (3) are computed from AMICS by the following equations:

$$F_{OM} = \frac{1}{M} \sum_{i=1}^M \sum_{j=1}^N \frac{A_{(OM)ij}}{A_{Ti}} \quad (10)$$

and

$$F_{Clays} = \frac{1}{M} \sum_{i=1}^M \sum_{j=1}^N \frac{A_{(Clays)ij}}{A_{Ti}} \quad (11)$$

where $A_{(OM)ij}$ is the area of OM particle j in image i , A_{Ti} is the total area of image i , N is the total number of particles analyzed per image, and M is the total number of images analyzed per sample.

In the calculation of F_{OM} and F_{Clays} , the areas of OM and clay particles that are not adjacent to accessible void spaces and, thus, may never be exposed to CO_2 for potential adsorption in a real matrix are included in the calculation, but these inaccessible fractions are removed subsequently by the efficiency factors associated with CO_2 adsorption on OM and clay particles. As discussed earlier, the SBA-derived efficiency factors represent only the fraction of OM or clay particles surfaces that are exposed to accessible pore or fracture spaces, thus, effectively precluding any inaccessible OM or clay particle contributions.

4.4. Maximum mass of CO_2 adsorbed by each component

The maximum mass of CO_2 adsorbed by each component (e.g., M_{OMCO_2} or $M_{ClaysCO_2}$) is determined from CO_2 adsorption analyses on "pure" component samples that are isolated from the rock matrix. The mass determined this way on crushed particles represents an overestimation because some of the surfaces exposed to CO_2 in crushed sample experiments may never be exposed to CO_2 in the natural environment. However, the derived efficiency factors that require surfaces to be exposed to accessible pores or fractures in 2-D cross sections of natural samples effectively corrects the overestimation in maximum mass obtained from adsorption analyses. The choice of CO_2 adsorption model for the maximum mass analysis needs to be carefully examined to ensure that an appropriate model is used because sometimes monolayer adsorption described by Langmuir model may work but in some cases the adsorption may be multilayer. For example, Vermulen (2011) showed that a BET model was more suitable for describing CO_2

adsorption on crushed Barnett shale samples.

4.5. Key assumptions of the approach

The main assumptions of the proposed equation include:

- 1 The fraction of OM, clays, or other adsorbing solid phase components is calculated as a volume fraction based on a stereological approximation.
- 2 The efficiency factor associated with adsorption by a given mineral component (e.g., OM or clays) is assumed to be proportional to the fraction of the component's particle borders shared with accessible pores or fractures.
- 3 Other CO_2 uptake mechanisms such as carbonate dissolution/precipitation, solubility in formation fluids, and/or hydrocarbon fluids are different from a surface adsorption phenomenon and so are not considered in this equation.
- 4 CO_2 adsorption by other major mineral grains such as quartz and feldspars is assumed to be negligible.
- 5 Surface coverage by CO_2 molecules is assumed to be a non-competitive, monolayer adsorption process.
- 6 CO_2 adsorption by a given mineral component of the rock is assumed to be independent of other components, thus, the contributions can be accounted for by using an additive model.

By taking into consideration these key assumptions and also considering that OM and clays are the dominant adsorbing components of Bakken shales and similar organic-rich shale formations, the overall image-based estimation equation for the prospective CO_2 mass storage resource potential for organic-rich shale reservoirs is given as follows:

$$G_{\text{CO}_2} = V_e [\rho_{\text{CO}_2} \phi_{\text{tot}} E_\phi + M_{OMCO_2} F_{OM} E_{OM} + M_{ClaysCO_2} F_{Clays} E_{Clays}] \quad (12)$$

The additional potential CO_2 uptake mechanisms described in Assumption 3 involving solubility in formation fluids, carbonates, etc., can be accounted for by using the "Others" term in Eq. (3) if suitable formulations are derived. As mentioned earlier in the geologic CO_2 storage mechanisms section, solubility uptake pathways are more feasible in conventional sandstone reservoirs with relatively large pore spaces. The mineralization mechanism will also become important in carbonate-type reservoirs, where soluble CO_2 and the resultant acidic solution can create dissolution/precipitation events that further stores CO_2 in the form of minerals. Since solubility and mineralization mechanisms are not quite applicable to organic-rich shales, derivation of appropriate expressions to quantify their contributions to CO_2 storage is the subject of ongoing development efforts for application to relevant reservoir types.

A challenge to the image-based equation concept is the need to incorporate experimentally determined CO_2 adsorption data for relevant adsorptive components such as OM and clay minerals. These components are expected to be isolated from the rock matrix and tested as relatively pure components, a task that can be nontrivial in practice. In addition, the adsorption experiments are assumed to capture or require Langmuir monolayer adsorption on the surfaces of crushed particles of OM or clays. Although Langmuir adsorption kinetics may be a reasonable approximation, the real adsorption behavior may be more complicated. Another technical challenge is the determination of connected versus nonconnected pore and fracture void spaces in the matrix. Advanced image analysis techniques applied to 3-D imagery can be used to differentiate between connected and nonconnected porosity; however, there is a trade-off between acquiring 3-D imagery that has a high enough resolution to resolve features of interest versus analyzing sample volumes that are so small that scaling up to the core-scale and reservoir-scale becomes challenging.

Table 1
Physical properties of CO₂ and Bakken Formation Shales.

| Property | Value | Comment |
|----------------------------|-------------------------|---|
| Area | 520,000 km ² | Approximate area |
| UBS thickness | 6 m | Maximum thickness (Hester and Schmoker, 1985) |
| MB3 thickness | 21 m | Maximum thickness (Hester and Schmoker, 1985) |
| LBS thickness | 14 m | Maximum thickness (Hester and Schmoker, 1985) |
| Total thickness | 43 m | Maximum thickness (Hester and Schmoker, 1985) |
| Density (shale) | 2300 kg/m ³ | Hester and Schmoker, 1985 |
| Density (MB3) | 2640 kg/m ³ | Hester and Schmoker, 1985 |
| Density (CO ₂) | 680.2 kg/m ³ | Linear interpolation from Span & Wagner tables at 5000 psi and 110 °C for approximate Bakken reservoir conditions |

5. Preliminary estimates of the prospective CO₂ storage potential for bakken shales

To illustrate the application of the newly developed equation, the data generated from 3 UBS and 3 LBS samples was used to obtain a preliminary estimate of the prospective CO₂ storage potential for the Bakken shales. Although the sample set utilized in this study is small and does not represent the entire Bakken formation, it facilitates a discussion of the potential impact of the equation as well as assists in the development of a roadmap for future improvement. In addition, the high heterogeneity of Bakken formation mineralogy both laterally and vertically suggests a larger sample set that is carefully selected would be required for a more representative estimate of the efficiency factors and, hence, an overall estimate of prospective CO₂ storage potential for Bakken shale on a regional scale.

The relevant physical properties of the Bakken Formation and CO₂ are summarized in Table 1. The density of CO₂ at Bakken reservoir conditions (~5000 psi and 110 °C) was calculated as a linear interpolation from Span & Wagner Tables (Span and Wagner, 1996). The net effective formation volume (V_e) was calculated by making an assumption that only about 20 % of the total formation area in Table 1 would be accessible for CO₂ storage; i.e., E_A = 0.2. Because the thickness of the shale units is small, a conservative estimate of potentially safe storage height of 3% was assumed, which gives E_h = 0.03. Other calculated parameters: efficiency factors, fractions of OM and clay minerals, and total porosity (including nano-/micro-fractures) are presented in Table 2. The fractions of OM (F_{OM}) and clay minerals (F_{Clays}) were obtained from the AMICS program (Gloy, 2019; Bruker, 2019). As discussed earlier, the AMICS program is an advanced mineral identification and characterization software that is capable of quantifying the mineralogy on a particle-by-particle basis based on 2-D particle areas. The results are then output as a mineral map and the associated table of quantified phases as illustrated in Fig. 6. To demonstrate the quality of the AMICS phase identification and quantification, the mineral map in Fig. 6 is compared with its corresponding BSE map; which shows good agreement in the resolution of the mineral grains. Observed mineral fractions vary between the samples which is typical for Bakken formation samples as reported by others in the literature (Lei, 2016). The mineral content variability also underscores the high degree of heterogeneity for Bakken shales.

The efficiency factors for CO₂ adsorption on OM (E_{OM}) and clay minerals (E_{Clays}) were calculated using the AIA protocol and the SBA

approach discussed in Section 3. The SBA routine basically computes the fraction of an OM particle border shared with connected porosity and then obtains an average of the shared border segments over all OM particles in a given image. Finally, the overall average over all images processed for a given sample yields the estimated efficiency factors for CO₂ adsorption onto OM. A similar analysis carried out on clay mineral particles gives an estimate of the efficiency factor for CO₂ adsorption on clay mineral surfaces.

The total porosity for each shale sample shown in Table 2 was determined from AIA using high resolution FESEM images at 3000x and at 20,000x or other suitable higher magnification. At 3000x most of the nanoporosity within OM is not well resolved spatially and, thus, is not quantified. Consequently, higher magnification images were obtained to facilitate the resolution of nanoporosity and nanofractures within OM. The porosity at higher magnification was then corrected for magnification differences and added to the porosity obtained at 3000x to obtain the total porosity of the sample.

5.1. Estimation of M_{OMCO₂} and M_{ClaysCO₂}

Ideally, the maximum mass of CO₂ adsorbed per unit volume of OM (M_{OMCO₂}) and clay (M_{ClaysCO₂}) surfaces is envisioned to be determined by performing CO₂ adsorption experiments (e.g., based on Langmuir or BET model) on fractions of clay minerals and OM that are isolated from the shale matrix. Although such experiments on isolated clays and OM fractions were beyond the scope of this work, there was some data on Langmuir adsorption on unseparated middle Bakken (MB3) and shale samples. Given that the MB3 samples typically have negligible OM content, CO₂ adsorption on MB3 samples would be dominated by clays and negligible contribution from OM. Thus, M_{ClaysCO₂} was estimated to be proportional to the mass of CO₂ adsorbed on the unseparated MB3 sample. Unlike the MB3, CO₂ adsorption on shale samples is due to both clay minerals and OM as the dominant contributions. As a result, M_{OMCO₂} was estimated as the difference in the asymptotic CO₂ adsorption masses between unseparated shale and MB3 obtained from their corresponding Langmuir CO₂ adsorption isotherms. Fig. 7 shows an example Langmuir isotherm that was obtained for an MB3 and a LBS sample. The M_{OMCO₂} and M_{ClaysCO₂} values used in the calculations reported herein are based on averages from two LBS samples, 3 MB3 samples, and 3 UBS samples. The M_{ClaysCO₂} value was determined to be 3.71 kg – CO₂/m³-rock and the M_{OMCO₂} values were 28.27 kg – CO₂/m³-rock and 20.97 kg – CO₂/m³-rock for the UBS and LBS, respectively.

5.2. Estimation of E_φ and prospective CO₂ storage

The efficiency factor associated with free phase storage is divided into E_{φeff}, which is the ratio of connected-to-total void volume and E_D, which is the reservoir fluid displacement efficiency. To illustrate the application of the proposed equation, the value of E_D = 0.074 was obtained from the literature (IEAGHG, 2014). Because of limited resources for this work, a procedure for distinguishing between connected and nonconnected porosity was not implemented to calculate effective porosity. However, Pang et al. (2017) have reported laboratory

Table 2
Calculated parameters for Bakken Formation Shale samples.

| Well | Lithofacies | E _{Clays} | E _{OM} | F _{Clays} | F _{OM} | Total porosity (%) |
|--------|-------------|--------------------|-----------------|--------------------|-----------------|--------------------|
| 22,388 | UBS | 0.00013 | 0.024 | 0.27 | 0.12 | 1.31 |
| 22,388 | LBS | 0.00015 | 0.026 | 0.38 | 0.11 | 1.78 |
| 16,974 | UBS | 0.0055 | 0.083 | 0.06 | 0.06 | 2.22 |
| 16,974 | LBS | 0.0014 | 0.038 | 0.30 | 0.07 | 0.29 |
| 18,829 | UBS | 0.00055 | 0.013 | 0.32 | 0.40 | 0.30 |
| 18,829 | LBS | 0.00027 | 0.032 | 0.49 | 0.04 | 1.32 |

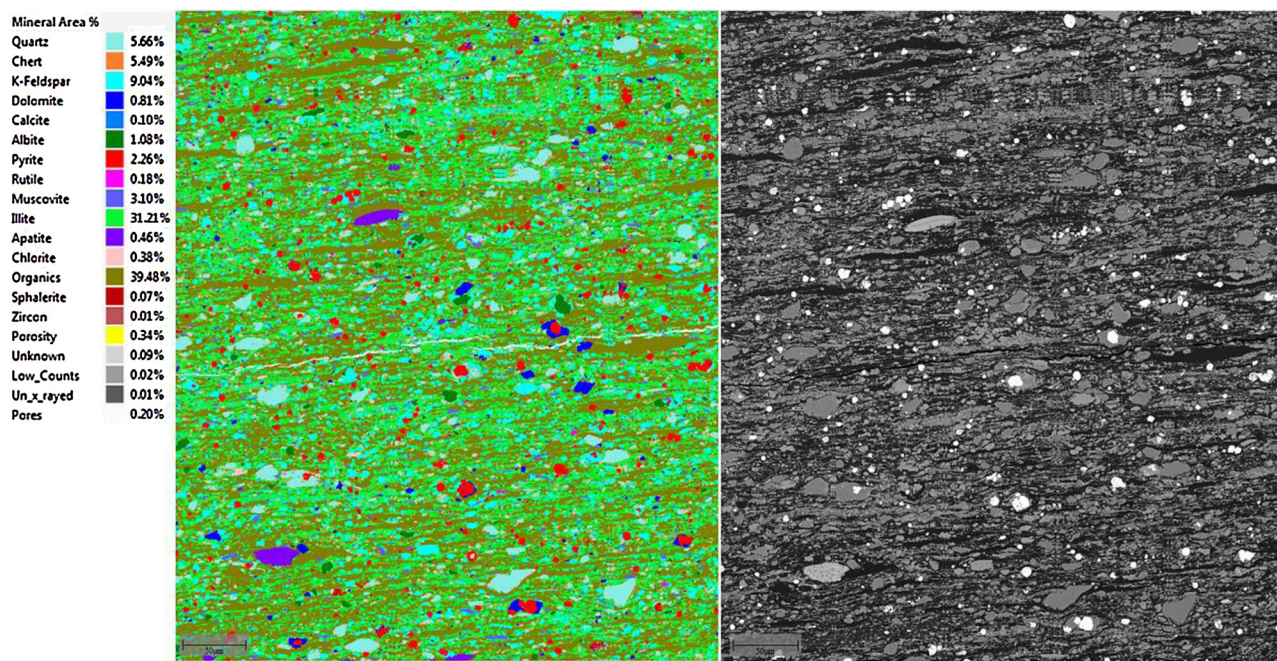


Fig. 6. AMICS mineral map of Upper Bakken shale compared to its corresponding BSE map.

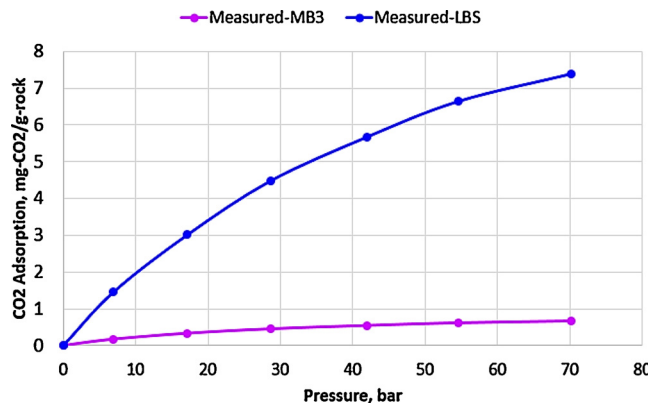


Fig. 7. Langmuir adsorption isotherms of MB3 and LBS sample.

Table 3
Calculated prospective CO₂ storage potential at low and high target $E_{\phi\text{eff}}$ levels for Bakken Formation Shale samples.

| Well | Lithofacies | Low (million tons) | High (million tons) |
|--------|-------------|--------------------|---------------------|
| 22,388 | UBS | 18 | 52 |
| 22,388 | LBS | 42 | 119 |
| 16,974 | UBS | 20 | 53 |
| 16,974 | LBS | 42 | 119 |
| 18,829 | UBS | 20 | 53 |
| 18,829 | LBS | 40 | 118 |

measured effective porosity fractions ($E_{\phi\text{eff}}$) for 5 different shale samples at 4000 psi in the range 0.016–0.048. These end point effective porosity values were used as Low and High targets and coupled with other calculated parameters and physical constants to obtain a range of prospective CO₂ storage resource potential for the Bakken shales shown in Table 3.

The results in Table 3 show that the average low target prospective CO₂ storage resource potential for the UBS is about 19 million tons, compared to 41 million tons for the LBS. The average high target levels are 54 and 119 million tons for the UBS and LBS, respectively. Thus, the

LBS demonstrate about 65 % more storage resource potential than the UBS for the samples studied. Additional comparisons of the amount of CO₂ adsorbed onto OM versus clays showed that OM can adsorb CO₂ better than clays by about 1–3 orders of magnitude. That is a direct consequence of 1–2 orders of magnitude lower E_{Clays} vs E_{OM} (Table 2). Clay mineral particle borders are shared with or exposed to a connected pore or fracture space to much lesser extent compared to OM. For example, the calculations in the Appendix A show that the amount of CO₂ adsorbed on OM is about 2 orders of magnitude larger than for clays for the UBS sample. Although these results are promising for unfractured shale samples, it should be noted that these are not optimal for the respective lithofacies and certainly are not representative of Bakken regional prospective CO₂ storage resource potential. The values obtained in this study were derived from a limited number of samples for the primary purpose of illustrating the newly-developed image-based equation for estimating the prospective CO₂ storage resource potential for shales. However, the results are encouraging and serve as a useful starting point for future investigations to better refine this approach and to expand the effort to regional scale.

6. Conclusions

This paper discusses an image analysis approach to further expand the volumetric equation for estimating the CO₂ storage resource potential for shale formations. The proposed equation enhances the volumetric equation methodology by systematically deriving expressions for calculating efficiency factors for clay minerals and OM based on analysis of high-resolution images obtained from organic-rich shales of the Bakken Formation. By deriving formation efficiency factors using images obtained from reservoir samples, more realistic efficiency factors can be determined for estimating the prospective CO₂ mass storage resource potential for shale reservoirs. The equation is also structured so that other potential CO₂ uptake mechanisms can be fully incorporated if appropriate formulations are derived, thus, retaining the flexibility to be applied to other types of reservoirs by adapting to the specific reservoir parameters/characteristics.

Preliminary data used to illustrate the newly-developed equation show that the UBS may have a lower prospective CO₂ storage resource potential than the LBS by about 65 %. However, these results are not

optimal for each lithofacies and are not at Bakken regional scale, but are encouraging for unfractured shale samples and serve as a useful starting point for future evaluations at the regional scale.

Declaration of interest

The authors declare no known competing financial interest or personal relationships that could have any influence on the work reported in this paper.

CRediT authorship contribution statement

Alexander Azenkeng: Conceptualization, Methodology, Investigation, Data curation, Formal analysis, Validation, Writing - original draft. **Blaise A.F. Mibeck:** Methodology, Data curation, Formal

analysis. **Bethany A. Kurz:** Supervision, Methodology, Writing - review & editing. **Charles D. Gorecki:** Methodology, Project administration, Funding acquisition. **Evgeniy M. Myshakin:** Writing - review & editing. **Angela L. Goodman:** Writing - review & editing. **Nicholas A. Azzolina:** Writing - review & editing. **Kurt E. Eylands:** Writing - review & editing, Methodology, Validation. **Shane K. Butler:** Writing - review & editing, Methodology. **Sean Sanguinito:** Writing - review & editing.

Acknowledgement

This work was performed with support from the U.S. Department of Energy (DOE) National Energy Technology Laboratory Cooperative Agreement No. DE-F0024233. However, any opinions, findings, conclusions, or recommendations expressed herein are those of the authors (s) and do not necessarily reflect the views of DOE.

Appendix A

An illustration of the developed equation

This Appendix provides an illustration of the steps taken in the calculation of G_{CO_2} using the equation presented in the main text where the prospective CO₂ storage resource potential for Bakken shales is given by

$$G_{CO_2} = V_e [\rho_{CO_2} \phi_{tot} E_\phi + M_{OMCO_2} F_{OM} E_{OM} + M_{ClaysCO_2} F_{Clays} E_{Clays}] \quad (A1)$$

The terms that need to be calculated include effective formation volume (V_e), free-phase storage term ($\rho_{CO_2} \phi_{tot} E_\phi$), CO₂ adsorbed onto OM ($M_{OMCO_2} F_{OM} E_{OM}$), and CO₂ adsorbed onto clays ($M_{ClaysCO_2} F_{Clays} E_{Clays}$).

Effective formation volume

The effective formation volume is given by

$$V_e = E_A \times A \times E_h \times h \quad (A2)$$

This example is based on the UBS unit with a total thickness of 6 m as presented in the text. The E_A and E_h values were also given in the text as 0.2 and 0.03, respectively. With an approximate Bakken formation area of about 520,000 km² (5.2×10^{11} m²), the effective volume is given by

$$V_e = 0.2 \times 5.2 \times 10^{11} \text{ m}^2 \times 0.03 \times 6 \text{ m} = 18,720,000,000 \text{ m}^3.$$

Free-phase storage (FPS)

The free-phase storage (FPS) and the associated efficiency factors are defined by the following equations:

$$FPS = \rho_{CO_2} \phi_{tot} E_\phi \quad (A3)$$

$$E_\phi = E_{\phi_{eff}} E_D \quad (A4)$$

$$E_{\phi_{eff}} = \frac{\phi_{con}}{\phi_{tot}} \quad (A5)$$

By substituting Eqs. (A4) and (A5) into Eq. (A3), the FPS is given by

$$FPS = \rho_{CO_2} \phi_{con} E_D \quad (A6)$$

The density of CO₂ at Bakken reservoir conditions (~5000 psi, ~100 °C) was estimated using a linear interpolation of Span and Wagner Tables as 680.2 kg/m³ (Span and Wagner, 1996) and E_D was taken from literature as 0.074 (IEAGHG, 2014). While the routine to distinguish between connected and nonconnected porosity is being developed, potential low and high connected porosity fractions for shales were obtained from the literature (Pang et al., 2017) as 0.016 and 0.048, respectively. By substituting the CO₂ density, low and high target values for connected (total effective) porosity, and the volumetric displacement value, the estimated free-phase storage for the UBS was obtained as

$$FPS_{Low} = 680.2 \text{ kg/m}^3 \times 0.016 \times 0.074 = 0.81 \text{ kg CO}_2/\text{m}^3$$

$$FPS_{High} = 680.2 \text{ kg/m}^3 \times 0.048 \times 0.074 = 2.42 \text{ kg CO}_2/\text{m}^3$$

CO₂ adsorbed onto OM

The amount of CO₂ adsorbed onto OM is given by

$$M_{OMCO_2} F_{OM} E_{OM} \quad (A7)$$

The calculation of maximum mass of CO₂ (M_{OMCO_2}) from Langmuir analysis, total fraction of OM (F_{OM}) using AMICS program, and the efficiency

factor for adsorption onto OM (E_{OM}) using the SBA method are explained in the text. The values of these parameters for the UBS sample are $M_{OMCO_2} = 28.27 \text{ kg CO}_2/\text{m}^3$, $F_{OM} = 0.12$, and $E_{OM} = 0.024$. By substituting these values into Eq. (A7) gives

$$\text{CO}_2\text{Ads}_{\text{OM}} = 28.27 \text{ kg/m}^3 \times 0.12 \times 0.024 = 0.081 \text{ kg CO}_2/\text{m}^3$$

CO₂ adsorbed onto clays

The amount of CO₂ adsorbed onto clays is given by

$$M_{\text{ClaysCO}_2} F_{\text{Clays}} E_{\text{Clays}} \quad (\text{A8})$$

The calculation of maximum mass of CO₂ (M_{ClaysCO_2}) from Langmuir analysis, total fraction of OM (F_{Clays}) using AMICS program, and the efficiency factor for adsorption onto clays (E_{Clays}) using the SBA method are explained in the text. The values of these parameters for the UBS are $M_{\text{ClaysCO}_2} = 3.71 \text{ kg CO}_2/\text{m}^3$, $F_{\text{Clays}} = 0.27$, and $E_{\text{Clays}} = 0.00013$. By substituting these values into Eq. (A8) gives

$$\text{CO}_2\text{Ads}_{\text{Clays}} = 3.71 \text{ kg CO}_2/\text{m}^3 \times 0.00013 \times 0.27 = 0.00013 \text{ kg CO}_2/\text{m}^3$$

Substitution of the values for all the parameters calculated above into Eq. (A1) and applying the conversion from kg – CO₂ to tons – CO₂ (1 kg = 0.00110231 t), the total estimated low and high prospective CO₂ storage resource potential for the UBS as an example are given by

$$\begin{aligned} G_{\text{CO}_2\text{Low}} &= V_e(FPS_{\text{Low}} + \text{CO}_2\text{Ads}_{\text{OM}} + \text{CO}_2\text{Ads}_{\text{Clays}}) \\ &= 18,720,000,000 \text{ m}^3 (0.81 \text{ kg CO}_2/\text{m}^3 + 0.081 \text{ kg CO}_2/\text{m}^3 + 0.00013 \text{ kg CO}_2/\text{m}^3) \\ &= 18.3 \text{ million tons CO}_2. \end{aligned}$$

Similarly, the high estimate is given by

$$\begin{aligned} G_{\text{CO}_2\text{High}} &= V_e(FPS_{\text{High}} + \text{CO}_2\text{Ads}_{\text{OM}} + \text{CO}_2\text{Ads}_{\text{Clays}}) \\ &= 18,720,000,000 \text{ m}^3 (2.42 \text{ kg CO}_2/\text{m}^3 + 0.081 \text{ kg CO}_2/\text{m}^3 + 0.00013 \text{ kg CO}_2/\text{m}^3) \\ &= 51.5 \text{ million tons CO}_2. \end{aligned}$$

Appendix B. Supplementary data

Supplementary material related to this article can be found, in the online version, at doi:<https://doi.org/10.1016/j.ijggc.2020.103038>.

References

- Bachu, S., Bonjoly, D., Bradshaw, J., Burruss, R., Holloway, S., Christensen, N.P., Mathiassen, O.M., 2007. CO₂ storage capacity estimation—methodology and gaps. *Int. J. Greenh. Gas Control* 1, 430–443.
- Bruker, 2019. M4 TORNADO^{AMICS} – Automated mineral analyzer for mining and geosciences. Instrument Brochure: www.bruker.com/fileadmin/user_upload/8-PDF-Docs/X-rayDiffraction_ElementalAnalysis/mXRF/Brochures/Bro_m4_amics_8p_en_lores.pdf (Accessed April 2019).
- Busch, A., Alles, S., Gensterblum, Y., Prinz, D., Dewhurst, D.N., Raven, M.D., Stanjek, H., Krooss, B.M., 2008. Carbon dioxide storage potential of shales. *Int. J. Greenh. Gas Control* 29, 297–308.
- Chadwick, R.A., Zweigel, P., Gregersen, U., Kirby, G.A., Holloway, S., Johannessen, P.N., 2004. Geological reservoir characterization of a CO₂ storage site—the Utsira Sand, Sleipner, northern North Sea. *Energy Procedia* 29, 1371–1381.
- Chareonsuppanimit, P., Mohammad, S.A., Robinson, R.L., Gasem, K.A.M., 2012. High-pressure adsorption of gases on shales—measurements and modeling. *Int. J. Coal Geol.* 95, 34–46.
- Furre, A.-K., Eiken, O., Alnes, H., Veatvne, J.N., Kiær, A.K., 2017. 20 years of monitoring CO₂ injection at Sleipner. *Energy Procedia* 114, 3916–3926.
- Giliciz, A., Bodí, T., 2012. Measurement of porosity and gas permeability of tight rocks by the pulse decay method. *Geosci. Eng.* 1, 65–74.
- Gloy, G., 2019. High speed differentiation of mineral phases of similar BSE intensity with AMICS. Application Note # EDS-16: www.bruker.com/products/x-ray-diffraction-and-elemental-analysis/eds-wds-ebsd-sem-micro-xrf-and-sem-micro-ct/quantax-eds-for-sem/amics-software.html (Accessed February 2019).
- Goodman, A., Fukai, I., Dilmore, R., Frailey, S., Bromhal, G., Soeder, D., Gorecki, C., Peck, W., Rodosta, T., Guthrie, G., 2014. Methodology for assessing CO₂ storage potential of organic-rich shale formations. *Energy Procedia* 63, 5178–5184.
- Gundersen, H.J.G., Jensen, E.B., 1987. The efficiency of systematic sampling in stereology and its prediction. *J. Microsc.* 147, 229–263.
- Hamling, J.A., Gorecki, C.D., Klapperich, R.J., Saini, D., Steadman, E.N., 2013. Overview of the Bell Creek combined CO₂ storage and CO₂ enhanced oil recovery project. *Energy Procedia* 37, 6402–6411.
- Hendricks, K., 2009. Experiences in the salt creek field CO₂ flood. In: Presented at the 5th Annual Wellbore Integrity Network. May 13–14, Calgary, Alberta, Canada. Available online at <https://ieaghg.org/docs/wellbore/webi05%20pres/2009%20Wellbore%20Integrity%20Network.pdf> (Accessed February 2019).
- Hester, T.C., Schmoker, J.W., 1985. Selected Physical Properties of the Bakken formation and Montana part of the Williston Basin. Interior – USGS, Reston VA. G84186.
- Available online at https://store.usgs.gov/assets/mod/storefiles/PDF/OC-126_ND_MT_Selected_Physical_Properties_Bakken_Formation_1985.pdf (accessed 2/19/2019).
- Howard, C.V., Reed, M.G., 1998. Unbiased Stereology—Three Dimensional Measurement in Microscopy. Bios Scientific Publishers, Oxford.
- IPCC—Intergovernmental Panel on Climate Change, 2005. Chapter 5 In: Metz, B., Davidson, O., de Coninck, H.C., Loos, M., Meyer, L.A. (Eds.), Special Report on Carbon Dioxide Capture and Storage. Cambridge University Press, Cambridge, UK and New York, NY, USA, pp. 195–276.
- IEAGHG, 2014. CO₂ storage efficiency in deep saline formations: A comparison of volumetric and dynamic storage estimation methods. 2014/09.
- King, G.E., 2010. Thirty years of gas shale fracturing—what have we learned? In: Society of Petroleum Engineers, Annual Technical Conference and Exhibition. September 19–22, Florence, Italy, SPE 133456.
- Lei, M., 2016. An Examination of the Mineralogy and Lithology of the Bakken Shale With Implications Upon the Bakken Petroleum System, Southeastern Saskatchewan. Master's Thesis. Faculty of Graduate Studies and Research, University of Regina, Canada.
- Levine, J.S., Fukai, I., Soeder, D.J., Bromhal, G., Dilmore, R.M., Guthrie, G.D., Rodosta, T., Sanguinito, S., Frailey, S., Gorecki, C., Peck, W., Goodman, A.L., 2016. U.S. DOE NETL methodology for estimating the prospective CO₂ storage resource of shales at the national and regional scale. *Int. J. Greenh. Gas Control* 51, 81–94.
- Liu, F., Ellett, K., Xiao, Y., Rupp, J.A., 2013. Assessing the feasibility of CO₂ storage in the New Albany shale (Devonian-Mississippian) with potential enhanced gas recovery using reservoir simulation. *Int. J. Greenh. Gas Control* 17, 111–126.
- Myshakin, E.M., Saidi, W.A., Romanov, V.N., Cygan, R.T., Jordan, K.D., 2013. Molecular dynamics simulations of carbon dioxide intercalation in hydrated Na-Montmorillonite. *J. Phys. Chem. C* 117, 11028–11039.
- Norris, S.O., Scherlin, J.M., Mukherjee, J., Vanderwal, P.G., Abbas, S., Nguyen, Q.P., 2014. CO₂ foam pilot in salt creek field, Natrona County, WY, phase II – diagnostic testing and initial results. In: Presented at the SPE Annual Technical Conference and Exhibition. October 27–29, Amsterdam, The Netherlands, SPE-170729-MS.
- Otsu, N., 1979. A threshold selection method from gray-level histograms. *IEEE Trans. Syst. Man Cybern.* 9, 62–66.
- Pang, Y., Soliman, M.Y., Deng, H., Emadi, H., 2017. Analysis of effective porosity and effective permeability in shale-gas reservoirs with consideration of gas adsorption and stress effects. In: Presented at The SPE Low Perm Symposium. Denver, May 5 – 6, 2016. Available online at <https://www.onepetro.org/journal-paper/SPE-180260-PA> (Accessed 11 November 2019).
- Petroleum Technology Research Center, 2019. The IEAGHG Weyburn-Midale CO₂ Monitoring and Storage Project. Available online at <https://ptrc.ca/projects/weyburn-midale> (accessed 2/11/2019).

- Preston, C., Monea, M., Jazrawi, W., Brown, K., Whittaker, S., White, D., Law, D., Chalaturnyk, R., Rostro, B., 2005. IEA GHG weyburn CO₂ monitoring and storage project. *Fuel Process. Technol.* 86, 1547–1568.
- Rasband, W.S., 2016. ImageJ. U. S. National Institutes of Health, Bethesda, Maryland, USA 1997–2016. <https://imagej.nih.gov/ij/>.
- Ringrose, P.S., Mathieson, A.S., Wright, I.W., Selama, F., Hansen, O., Bissell, R., Saoula, N., Midgley, J., 2013. The In Salah CO₂ storage project—lessons learned and knowledge transferred. *Energy Procedia* 37, 6226–6236.
- Rodosta, T.D., Litynski, J.T., Plasynski, S.I., Hickman, S., Frailey, S., Myer, L., 2011. U.S. Department of Energy's site screening, site selection, and initial characterization for storage of CO₂ in deep geological formations. *Energy Procedia* 4, 4664–4671.
- Schindelin, J., Arganda-Carreras, I., Frise, E., Kaynig, V., Longair, M., Pietzsch, T., Preibisch, S., Rueden, C., Saalfeld, S., Schmid, B., Tinevez, J.-Y., White, D.J., Hartenstein, V., Eliceiri, K., Tomancak, P., Cardona, A., 2012. Fiji—an open-source platform for biological-image analysis. *Nat. Methods* 9 (7), 676–682.
- Shi, J.-Q., Imrie, C., Sinayuc, C., Durucan, C., Korre, A., Eiken, O., 2013. Snøhvit CO₂ storage project—assessment of CO₂ injection performance through history matching of the injection well pressure over a 32-months period. *Energy Procedia* 37, 3267–3274.
- Sommer, C., Strähle, C., Köthe, U., Hamprecht, F.A., 2011. Ilastik: interactive learning and segmentation toolkit. Eighth IEEE International Symposium on Biomedical Imaging (ISBI), Proceedings 230–233.
- Span, R., Wagner, W., 1996. A new equation of state for carbon dioxide covering the fluid region from the triple-point temperature to 1100 K at pressures up to 800 MPa. *J. Phys. Chem. Ref. Data* 25, 1509. <https://doi.org/10.1063/1.555991>.
- Tao, Z., Clarens, A., 2013. Estimating the carbon sequestration capacity of shale formations using methane production rates. *Environ. Sci. Technol.* 47, 11318–11325.
- Torp, T.A., Gale, J., 2004. Demonstrating storage of CO₂ in geological reservoirs—the Sleipner and SACS projects. *Energy* 29, 1361–1369.
- Vermylen, J.P., 2011. Geomechanical Studies of the Barnett Shale. Doctoral dissertation, Stanford University, Texas, USA.
- Watney, W.L., 2016. Horizontal drilling – technology review, current applications, and its future in developing Kansas' petroleum resources: Kansas Geological Survey, Lawrence, KS 66047. Available online at www.kgs.ku.edu/PRS/Unger/Watney-KBA-KIOGA-Horizontal_Drilling.pdf (Accessed January 2016).
- Weibel, E.R., 1979. *Stereological methods: Practical Methods for Biological Morphometry*. Academic Press, London.